

RESOLUTION ENHANCEMENT ASPECTS
IN B - SCAN ULTRASONOGRAPHY

SATPAL SINGH

Thesis submitted to

INDIAN INSTITUTE OF TECHNOLOGY
NEW DELHI

for the award of degree of
DOCTOR OF PHILOSOPHY

Center for Biomedical Engineering
Indian Institute of Technology
New Delhi 110016

OCTOBER, 1986

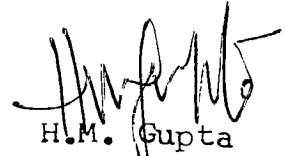
CERTIFICATE

This is to certify that the dissertation,
"Resolution Enhancement Aspects in B - Scan
Ultrasonography" being submitted by Mr. Satpal Singh
for the award of the degree of Doctor of Philosophy
at the Indian Institute of Technology, Delhi, is a
record of bonafide research work carried out by him
under our supervision and guidance.

This dissertation has reached the standard
fulfilling the requirements of the regulations relating
to the degree. The results contained in this thesis
have not been submitted to any other University or
Institute for the award of any degree or diploma.



S.N. Tandon
Professor, Centre for Biomedical
Engineering
Indian Institute of Technology,
New Delhi 110016,
INDIA



H.M. Gupta
Professor
Department of Electrical
Engineering
Indian Institute of Tech.,
New Delhi 110016,
INDIA

Dated _____

ACKNOWLEDGEMENT

I express my deep sense of gratitude to Prof. S.N. Tandon and Prof. H.M. Gupta for their invaluable guidance and encouragement during the course of this research. My special thanks are due to Dr. Tandon for introducing me to the field of Biomedical Engineering. I am grateful to Dr. Gupta for inculcating in me the analytical approach.

I express my sincere thanks to Dr. B. Bhattacharya with whom I took full liberty to discuss at length all sorts of problems that I encountered.

I am grateful to the faculty and all other members of the Centre for BME who participated in the various discussions and provided me with valuable suggestions from time to time. Notable mentions are Dr. D. Mohan, Dr. K.B. Sahai, Dr. M. Cauba, Dr. A.R. Ray, Dr. K.P. Kothiyal, Dr. Harpal Singh, Mr. S.M.K. Rahman and Mr. Dinesh Kant. I am also thankful to Prof. S. K. Guha for having brought me into the fold of Biomedical group at IIT Delhi.

I am thankful to Mr. N.D. Arora without whose help this thesis could not have been typed in its present form.

I am also grateful to my parents, but for whose support and encouragement, this work would not have been possible.

Finally, I must express my utmost thanks to my dear wife for bearing with me and allowing me sufficient time to work towards the completion of this work.

Satpal Singh

ABSTRACT

Ultrasonic B scan is a widely used non - invasive method for obtaining the cross sectional images of soft tissues. The diagnostic utility of a B scan image depends on its resolution or its ability to show up the details corresponding to the morphology of the tissue. The resolution in B scan is primarily limited due to lateral blurring and speckle. The former lowers the sharpness or contrast of the image and the latter manifests as a granular texture which tends to mask the true details of the tissue. This thesis is concerned with the improvement of resolution in B scan images in the presence of above degradations.

The loss in resolution due to lateral blurring results due to the non - zero beam spread used in B scan imaging. This is modelled as a convolution process. Therefore, the natural recourse to resolution improvement is by the process of deconvolution. The existing deconvolution techniques are computationally expensive and hence a new iterative technique with rapid convergence has been formulated. The computer simulation results have been presented to demonstrate the efficacy of the proposed technique.

The degradation due to speckle has been modelled as a complex interference phenomena. The study of various models show that the speckle depends amongst other factors, on the pulse used for echo imaging. The effect of pulse bandwidth and the use of FM pulses for speckle reduction have been investigated in this thesis. Computer simulation results have been presented to justify the use of wide

band FM pulses for speckle reduction. A comparative study between frequency compounding and axial compounding has been presented. It has been concluded that for a given time bandwidth product, axial compounding with wide band pulses is superior to frequency compounding.

An extension of the sequential mode of data acquisition and employing the method of backprojection for image reconstruction has also been investigated. A scheme utilising an analogue scan converter for speedy image reconstruction has been suggested. The resolution obtained by this method has been compared to the diffraction limited resolution obtained by other techniques .

Finally, the work presented in this thesis has been summarised and suggestions for further work have been given in the last chapter.

LIST OF SYMBOLS

The symbols used in the thesis represent the following unless stated otherwise.

- a_n amplitude of backscattered wave from the nth scatterer.
- A operator in Ch. III
Chirp rate in Ch. IV
- b inter element spacing
- $b_{i,n}$ time taken by the wave to travel from ith scatterer to the nth element of an array.
- $b_n(y_0, z_0)$ Backprojection at (y_0, z_0) from the nth element of array.
- B Bandwidth
- $B_0, B_k, B_0^*, B_k^* =$ Operators
- c Velocity of sound
- C Constraining Operator
- C_n arc of radius r_n from the nth element of linear array (or the nth position of a scanning transducer).
- d_n wave propagation time from the transducer to nth scatterer.

$d_{m, i}$	wave propagation time from the mth element of array to ith scatterer
$d(f, g)$	distance between elements f and g of a vector space.
D	aperture of a linear transducer.
$e(t)$	pulse envelope
$\{e_k\}$	error sequence in $[f_k]$, Eq. (3.4)
$\{e_{g,k}\}$	error sequence, eq. (3.7)
$E(\omega)$	Fourier transform of $e(t)$
$E\{ \}$	Expected value of quantity enclosed within the brackets
$f(n)$	signal
\underline{f}	signal vector
f_k	kth estimate of f
$f(r, \theta), f(y, z)$	= specimen reflectivity
$f_b(y_0, z_0)$	Image reconstruction at (y_0, z_0) by backproject:
$\{f_k\}$	sequence of f_k , for $k = 1, 2, 3, \dots$
$F(u)$	Fourier transform of $f(n)$
$F(U, V)$	Fourier transform of $f(y, z)$

$F(r, \bar{\phi})$	Fourier transform of $f(r, \theta)$ with respect to θ .
$F(\bar{\phi})$	$F(r, \bar{\phi})$ at a fixed value of r .
FM	Frequency modulation
$g(t)$	signal received by the transducer
$g_n(t)$	signal received by the n th element of a linear array.
$g(r, \theta)$	signal received from a range r when the transducer is directed at an angle θ .
$G(\omega)$	Fourier transform of $g(t)$
$G(r, \bar{\phi})$	Fourier transform of $g(r, \theta)$ with respect to θ
$G(\bar{\phi})$	$G(r, \bar{\phi})$ at a fixed value of r .
$h(n), h(\theta)$	blur function.
$h(y, z), h(r, \theta)$	= radiation spread function
$h(\underline{r}, t)$	acoustical impulse response of transducer
$h_{rx}(r, \theta)$	receive aperture function
$h_{tx}(r, \theta)$	transmit aperture function
H	distortion operator
\underline{H}	distortion matrix

$H(\mathbf{u})$	Fourier transform of $h(\mathbf{r})$
$H(r, \Phi)$	Fourier transform of $h(r, \theta)$ with respect to θ
$H(\Phi)$	$H(r, \Phi)$ at a fixed value of r .
inf	infimum
I	Identity operator
j	$\sqrt{-1} =$ complex quantity
k	wave number
k_c	denotes the complex wave number
L	Time delay for excitation between the successive elements of a linear array
LPF	low pass filter.
M	bound of operator T
n	noise
N	number of elements of a linear array
$p(t)$	pulse
$P(\omega)$	Fourier transform of $p(t)$
r	axial distance or range
\mathbf{r}	position vector

r_n	distance of the point of interest (y_0, z_0) from the n th element of a linear array
R	enhancement factor
R_f, R_g, R_p	Autocorrelations of functions f, g and p respectively
RHS	Right hand side
s_{cy}, s_{cz}	Speckle size along the y and z axes respectively
$s(t)$	effective backscatter strength, eqs. (2.81) and (2.82)
$s(r)$	equivalent specimen reflectivity at range r , eq. (4.2)
$s_n(r_n)$	equivalent specimen reflectivity at range r_n from the n th element of an array, eq. (6.4)
S	Vector space
SNR	Signal to noise ratio
t	time variable
T	pulse duration
T^k	Operator - in Ch. III only denotes an operator applied k times
T_c	correlation length along time axis, eq. (4.5)
U	spatial frequency along the y axis
$U_T(t)$	rectangular window, eq. (4.11)

W_B	lateral spread function width in a backprojected image eq. (6.37)
W_d	Lateral beam width at the focal point of a linear array.
W_s	Lateral spread function for a synthetic aperture technique.
W_y	lateral spread function width in a demodulated, backprojected image, eq. (6.46)
y	lateral axis coordinate
z	depth axis coordinate
z_{tr}	transition range

Greek and Special Symbols

α	Angular coordinate used as $f(r, \alpha)$ perturbation in H , eq (3.37) in Ch. III only.
θ, θ_n, ϕ	angular coordinate
ϕ	zero operator in Ch. III only
ϕ_n	phase of the n th backscattered wave
$\delta(\)$	kroncker delta function
ξ	perturbation in T , eq. (3.12) in Ch. III only

ϵ	belongs to
Φ	Fourier domain variable corresponding to θ .
λ	wavelength of ultrasound in the specimen at angular frequency ω
σ, σ_z	standard deviations of gaussian functions.
$\tau, \tau_n, \tau_{n,s}$	= time delays.
u	Fourier domain variable corresponding to variable n
μs	micro seconds
ω	angular frequency
∞	infinity
$ $	absolute value of quantity enclosed
$ $	norm of quantity enclosed
$\langle \rangle$	sample average of quantity enclosed
$*; f * h$	denotes convolution of f and h
T^*	superscript star denotes the perturbed quantity T in Ch. III only
f^*	superscript star denotes the complex conjugate of quantity f
\forall	for all

LIST OF FIGURES

- Fig. 2.1 B. Scan Imaging, (a) Linear Scan
(b) Sector Scan 8
- Fig. 2.2 The Radiation spread of the transducer
O is contained in the sector AOB. Q(r, α)
is an arbitrary scan point and $\alpha = \phi - \theta$ 17
- Fig. 2.3 $H(\phi)$ is the blur function. The noise
suppression filters $H_O(\phi)$, $H_G(\phi)$ and
 $H_B(\phi)$ correspond to the Wiener, Gaussian
and 1st order Butterworth filters respectively. 31
- Fig. 2.4 Acoustic speckle model. The convoluted
wavefront at the transducer is caused by
multiple scatterers, intervening media,
multiple reflections and other unknown
factors [Fig. 5 in [65]]. 46
- Fig. 2.5 The effective backscattering strength $s(t)$
is the summation of the backscattering
strengths of all the random scatterers
lying on the arc of radius $t \cdot c/2$ and
centre at O, the position of the transducer. 66
- Fig. 3.1 Region in the complex $H(u)$ plane for which
the iterative deconvolution technique
converges. [Fig. 1 in [96]]. 91

Fig. 3.2 (a) $f(n)$ is the original signal of interest and $g(n)$ is the blurred signal obtained on convolving $f(n)$ with a Gaussian blur function of standard deviation equal to six sampling intervals. (b), (c), (d): Restored signal $f_k(n)$ for $k = 1, 2, 3$. (b) SNR = ∞ . (c) SNR = 40 dB. (d) SNR = 28 dB.

93

Fig. 3.3 (a) Observed signal $g(n)$ of a gamma - ray spectrum [Fig. 7.a in [96]]. (b) Blur function $h(n)$ [Fig. 7.c in [96]]. (c) Restored signal after 20th iteration using the equation $f_{k+1} = \lambda \cdot g + (\delta - \lambda \cdot h) * C f_k$, with $\lambda = 2$ and C imposing both finite support and positivity constraint [Fig. 7.f in [96]]. (d) Results obtained with $\lambda = 1$ and no constraint applied (Van Citterts algorithm) [Fig. 7.d in [96]]. (e) Results obtained with $\lambda = 1$ and a finite support constraint. The region of support is $45 \leq n \leq 290$ [Fig. 7.e in [96]].

95

Fig. 3.4(a) Restored signal after the 4th iteration (the peak has been normalised to a maximum value of 1). Results were obtained by applying the proposed restoration technique along with the positivity constraint to the signal $g(n)$ in Fig. 3.3.a. Comparison with Fig. 3.3c reveals the fast convergence of the proposed technique (b) Restored signal after 4th iteration, obtained on using the proposed algorithm with no constraints involved Comparison with Fig. 3.3(d), (e) reveals the efficacy of the proposed algorithm.

98

- Fig. 3.5 (a) $f(n)$ is the original signal and $g(n)$ is obtained on convolving $f(n)$ with a cosine squared function of (3.65). (b), (c): Restored signal $f_k(n)$ for $k = 1, 2, 3$. (b) SNR = ∞ . (c) SNR = 28 dB 100
- Fig. 3.6 (a) Lateral point response in the field of the split aperture transducer [Curve x, Fig. 31.c in [18]]. (b) $g(n)$ is obtained by convolving $f(n)$ with $h(n)$ in (a), (c) (d): Restored signal $f_k(n)$ for $k = 1, 2, 3$ (c) SNR = ∞ . (d) SNR 28 dB. 102
- Fig. 3.7 (a) Measured lateral beam pattern at distance of 10 cm of a 5 MHz, spherically focussed circular aperture transducer of 12.7 mm diameter and 10 cm focal length [Fig. 3.7 in [163]]. (b) $g(n)$ is obtained by convolving $f(n)$ with $h(n)$ in (a). (c), (d): Restored signal $f_k(n)$ for $k = 1, 2, 3$ (c) SNR = ∞ . (d) SNR = 28 dB. 104
- Fig 4.1: RF pulse of duration T_p and frequency f_c in (a) and its spectrum in (b). 110
- Fig. 4.1 Interference of two backscattered waves delayed by $\lambda/2$ in (a) and by λ in (b). The tracings A show the reflected waves from a two point medium, B their resultant, C the full wave rectified output and D the low pass filtered version of C. 113

- Fig. 4.3 Sample pulse shapes with different Gaussian envelopes (a) $\sigma = 62.5 \mu\text{s}$ (b) $\sigma = 0.625 \mu\text{s}$. 127
- Fig. 4.4 Amplitude spectra of the pulse for different values of σ of the gaussian envelope. The tracings, A, B, C, D, E, F, G and H correspond to $\sigma = 62.5, 0.625, 0.416, 0.313, 0.208, 0.156, 0.104,$ and $0.078 (\mu\text{s})$ respectively. 128
- Fig 4.5: SNR vs $\sqrt{\text{Bandwidth}}$ for gaussian pulse shape 129
- Fig. 4.6 Amplitude spectra of $2 \mu\text{s}$ long FM pulses for Chirp rates (MHz / μs) of 0, 0.588, 1.2 and 1.8 are shown in tracings A, B, C and D respectively 132
- Fig 4.7: (a) SNR vs chirp rates for different pulse durations. The dashed curves show the SNR obtained on matched filtering before envelope detection. (b) SNR vs $\sqrt{\text{Bandwidth}}$ for $T = 2 \mu\text{s}$. 133
- Fig 4.8: Improvement in axial resolution on matched filtering for FM pulses of duration $3.5 \mu\text{s}$ and initial frequency 2 MHz. (a) and (c) are the received signal for chirp rates of 0 and $0.75 \text{ MHz}/\mu\text{s}$ respectively; (b) and (d) are their respective matched filter outputs. The boundary of the scattering region, indicated by the vertical arrow, is enhanced in (d). 134

- Fig 4.8: Improvement in axial resolution on matched filtering for FM pulses of duration $3.5 \mu\text{s}$ and initial frequency 2 MHz. (e) and (g) are the received signal for chirp rates of 1.5 and 2.25 MHz/ μs respectively; (f) and (h) are their respective matched filter outputs. The boundary of the scattering region, indicated by the vertical arrow, is enhanced in (f) and (h). 135
- Fig. 5.1 (a) Focussing of ultrasound using a linear array (b) Circular arcs over which the reflectivities of the specimen get integrated to yield the receive focus signal at $A(y_0, z_0)$. 140
- Fig. 5.2 (a) Reflective tomography, with data acquisition over a circular aperture. 154
(b) Reflective tomography using an array. The B scans obtained from different positions around the specimen are backprojected 155
- Fig. 5.3 Echo - imaging with a linearly scanned aperture; y_n is the position of a small element transducer. 159
- Fig. 5.4 The geometry of a point image obtained by backprojection of the demodulated observations. 164

- Fig. 5.5 The proposed backprojection scheme 169.
- Fig. 5.6 Receive beam patterns for a phase sensitive
imaging array in the absence A and in the
presence B of tissue inhomogeneties
[Fig. 8 in [85]]. 174
- Fig. 5.7 Receive beam patterns of phase insensitive
imaging systems in the absence A and presence
B of tissue inhomogeneties [Fig. 9 in [85]]. 175

CONTENTS

ABSTRACT		(i)
LIST OF SYMBOLS		(iii)
LIST OF FIGURES		(x)
<u>CHAPTER I:</u>	INTRODUCTION	1
<u>CHAPTER II:</u>	RESOLUTION ASPECTS IN B SCAN IMAGES	6
	2.1 Introduction	6
	2.2 Lateral Resolution in B Scans	16
	2.2.1 Blurring in B scans	16
	2.2.2 Restoration of B Scans	21
	2.2.3 The Deconvolution Techniques	33
	2.3 Ultrasonic Speckle	41
	2.3.1 Modelling of Speckle	42
	2.3.2 Reduction of Speckle	58
	2.4 Summary	68
<u>CHAPTER III:</u>	A DECONVOLUTION TECHNIQUE	71
	3.1 Introduction	71
	3.2 The Iterative Techniques	73
	3.2.1 A Generalized Approach	75
	3.2.2 Convergence	76
	3.2.3 Perturbation in the Operator T	77
	3.2.4 Noise Effects	78

3.3	The Proposed Technique	80
3.3.1	The Technique	80
3.3.2	Convergence	82
3.3.3	Perturbation in the Operator H	84
3.3.4	Noise Effects	87
3.4	Application to Deconvolution	89
3.4.1	Computational Results	90
3.5	Discussion	99

CHAPTER IV

A STUDY ON SPECKLE REDUCTION BY THE TECHNIQUES OF FREQUENCY COMPOUNDING AND AXIAL COMPOUNDING (TIME AVERAGING)

4.1	INTRODUCTION	108
4.2	SPECKLE DEPENDENCE ON PULSE	111
4.2.1	The Convolution model	111
4.2.2	The Bandwidth	114
4.2.3	The Autocorrelation	115
4.3	FREQUENCY COMPOUNDING	119
4.4	AXIAL COMPOUNDING	121
4.4.1	Speckle Reduction	121
4.4.2	Computer Simulations	123
	4.4.2.a Simulations for amplitude modulated gaussian pulses	125
	4.4.2.b Simulations for frequency modulated pulses	130
4.5	CONCLUSIONS	136

<u>CHAPTER V</u> :	HIGH SPEED HIGH RESOLUTION ULTRASONOGRAPHY	137
5.1	Introduction	137
5.2	Resolution Aspects in Various Echo Imaging Systems Using Ultrasound	138
5.2.1	Phased Array Focussing	138
5.2.2	Holographic Image Reconstruction	145
5.2.3	Synthetic Aperture Techniques	149
5.2.4	Synthetic Focussing	151
5.2.5	Reflective Tomography	153
5.3	A High Speed Resolution System	157
5.3.1	Backprojection Applied To Linear Scanning	158
5.3.2	The Proposed System	168
5.3.3	Speed Considerations	170
5.4	Discussion	173
<u>CHAPTER VI</u> :	CONCLUSIONS	177
	REFERENCES	183
	LIST OF RESEARCH PAPERS BASED ON Ph.D THESIS	206